

Phonons in MoSe₂/WSe₂ van der Waals heterobilayer

F. Mahrouche,^{1,2} K. Rezouali,¹ F. Zaabar,¹ and A. Molina-Sánchez³

¹*Laboratoire de Physique Théorique, Faculté des sciences exactes, Université de Bejaia, 06000 Bejaia, Algérie*

²*Departamento de Física Aplicada, Universidad de Alicante, 03690 San Vicente del Raspeig, Spain*

³*Institute of Materials Science (ICMUV), University of Valencia, Catedrático Beltrán 2, E-46980, Valencia, Spain*

We report first-principles calculations of the structural and vibrational properties of the synthesized two-dimensional van der Waals heterostructures formed by single-layers dichalcogenides MoSe₂ and WSe₂. We show that, when combining these systems in a periodic two-dimensional heterostructures, the intrinsic phonon characteristics of the free-standing constituents are to a large extent preserved but, furthermore, exhibit shear and breathing phonon modes that are not present in the individual building blocks. These peculiar modes depend strongly on the weak vdW forces and has a great contribution to the thermal properties of the layered materials. Besides these features, the departure of flexural modes of heterobilayer from the ones of its monolayer parents are also found.

I. INTRODUCTION

Comprised of one or several covalently bound sheets of atoms held together by van der Waals (vdW) forces, two-dimensional (2D) systems and layered weakly-bound structures thereof¹⁻³ have interesting properties that make them highly desirable in many fields. Besides their fascinating properties, they have the potential to sharply reduce the characteristic lengths of electronic devices thus opening up unprecedented perspectives in view of designing low-power devices such as ultra-thin-channel field-effect transistors and solar cells. The family of transition metal dichalcogenides (TMDs) is one of these engaging materials, consisting of atomically thin semiconductors of the type MX₂ where M is a transition metal atom (Mo or W, etc.) and X is a chalcogen atom (S, Se or Te). They exhibit small direct bandgaps lying in visible and near-IR ranges⁴ making them attractive shortly after they were isolated due to their unique physicochemical properties and potential applications in electronic and optoelectronic devices. For example, WSe₂ is used as field-effect transistors (FETs)⁵, logic-circuit integrations, and optoelectronic devices⁶, while MoSe₂ is used in field effect transistors⁷, solar cells and photoelectrochemical devices⁸⁻¹⁰.

Beyond 2D materials considered individually, composite systems stacks of different layers, called van der Waals heterostructures¹¹ are particularly attractive: They allow not only to modulate the properties of the materials, but also to further improve their performance. Recently, many efforts are devoted to investigate the different properties of a wealth of vdW hybrid heterostructures (vertical and lateral) such as MoSe₂/WSe₂¹², WSe₂/MoS₂¹³ MoS₂/h-BN/graphene¹⁴. In particular, many experimental and theoretical studies of the physical properties of MoSe₂/WSe₂ heterostructure have been done because of their potential for optoelectronic and electronic technologies and light harvesting applications.¹⁵⁻²⁰ Despite the effort devoted the study of the dynamical and vibrational properties of

the heterostructures based on the MoSe₂ and WSe₂ are scarce.

In this work, we investigate the structural and vibrational properties of MoSe₂/WSe₂ van der Waals heterostructures with a special focus on the observed inter-layer phonon modes in the studied systems. The phonon characteristics of the heterobilayer (HBL) are calculated in the framework of lattice dynamics theory using appropriate ab-initio methods. These present-day theories can compute phonons in many systems without any adjustable parameters making them complementary tools to the measurements. We explore emergent properties in the composite system that are absent in the individual layers. Our calculation reveals the existence of interlayer shear and breathing phonon modes in the heterobilayers. These peculiar phonons exist only in bilayer areas and are paramount to understand the different scattering mechanisms in layered 2D materials.

The manuscript is organized as follows. Descriptions of the computational methods are given in Section II. In Section III, we report and discuss our results, and finally we summarize our main conclusions.

II. METHODS

XSe₂ { X=Mo or W } are transition metal dichalcogenides consisting of covalently bound Se-X-Se sheets that are held together by van der Waals (vdW) forces as shown in Fig.1. Each one of these single layers consists of hexagonal plane of metallic X atoms sandwiched between two hexagonal planes of Se atoms bound with the metallic atoms in a trigonal-prism arrangement.

The unit cell is constructed by combining a 1 × 1 unit cell of monolayer MoSe₂ and 1 × 1 unit cell of WSe₂ sheet. The primitive lattice vectors spanning the heterobilayer supercell are chosen in commensuration with those of the isolated layers. The supercell containing 6 atoms is depicted in Fig.1. The determination of the equilibrium geometry of any structure constitutes the pivotal step before investigating phonons

or any other related physical properties. The calculations are carried out using density functional theory (DFT)^{21,22} as implemented in the open-source code QUANTUM ESPRESSO.²³ We adopted the Perdew-Burke-Ernzerhof exchange correlation functional.²⁴ The ionic potential has been modeled using Optimized Norm-Conserving Vanderbilt (ONCV) pseudopotentials.²⁵ To correctly describe the effect of dispersive forces, we employed the Tkatchenko-Scheffler (TS) dispersion corrections method²⁶ which has been demonstrated to give a reliable prediction for both interlayer distances and binding energies for vdW systems. The calculations were done in the supercell arrangement using a 80 Rydberg (Ry) plane-wave cutoff for the electronic wave function expansion. To maintain the periodicity along the direction perpendicular to the sheet, we used a vacuum of 18 Å. The first Brillouin zone is sampled with a $12 \times 12 \times 1$ Monkhorst-Pack grid²⁷ together with a simple Gaussian smearing in the electronic occupations of 0.02 Ry for single-layer and heterobilayer systems. This technique is also used to avoid the spurious interlayer interactions. The equilibrium atomic coordinates has been obtained fully minimizing unit cells using the calculated forces and stress on the atoms. The convergence criterion of self-consistent calculations for ionic relaxations is 10^{-10} eV between two consecutive steps. All atomic positions and unit cells are optimized until the atomic force convergence of 10^{-3} eV/Å were reached. The above criteria ensure the absolute value of stress is less than 0.01 kbar.

To benchmark our structural calculations, the lattice parameters, bond lengths, and bond angles of monolayers WSe₂ and MoSe₂ are determined beforehand and gathered in Table I. The calculated lattice constants are evaluated to be $a = 3.31$ Å for both monolayers MoSe₂ and WSe₂. The Mo–Se and W–Se bond lengths are calculated to be about 2.54 Å and 2.55 Å, respectively. The out-of-plane Se–Se bond lengths is evaluated to be 3.34 Å and 3.39 Å for MoSe₂ and WSe₂, respectively. The out-of-plane \angle SeMoSe and \angle SeWSe bond angles are calculated to be about 82.19° and 83.07°, respectively. Our results are in accordance with available theoretical and experimental data.^{28–30} For heterobilayer, the lat-

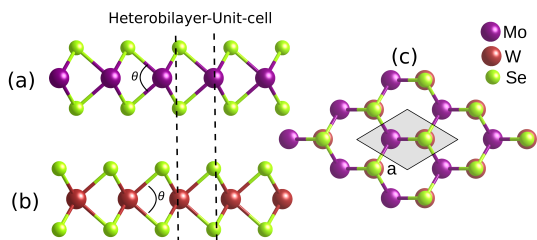


FIG. 1. (Color online) Side view and top view of atomic structures of van der Waals heterobilayer MoSe₂/WSe₂.

tice constant a is decreased when compared with that of isolated layers by about 0.6%. The Mo–Se and W–Se bond lengths are calculated to be about 2.53 Å which de-

creases by less than 0.8% than those of its parent layers reflecting the weak interlayer interaction. The interlayer distance d between MoSe₂ and WSe₂ monolayers is 3.22 Å. It should be noted that our structural forecasts are in good agreement with the theoretical data.³¹

The phonon characteristics of a given material are often described in the context of lattice dynamics theory by using appropriate first-principles methods. The inputs are the second interatomic force constants (IFCs). IFCs were calculated using density functional perturbation theory (DFPT).³² Non-analytical terms due to the Coulomb forces, Born charges, and dielectric constants are all gathered in the dynamical matrices for both the subunits and their descending heterobilayer. Phonon group velocity is calculated based on the phonon dispersion relation for each single mode. For the calculation of the harmonic IFCs, a Wigner-Seitz (primitive) equilibrium cell of each structure of interest is used. The harmonic IFCs were performed on $12 \times 12 \times 1$ \mathbf{k} point meshes for phonon calculations of single-layers and heterobilayer, with a simple Gaussian smearing in the electronic occupations of 0.02 Ry. The above samplings are sufficient to map out all the possible instabilities and offer well-converged phonon eigenvalues for all of the structures treated here.

Material	a	d_{X-Se}	d_{Se-Se}	d	\angle SeMoSe	\angle SeWSe
MoSe ₂	3.31	2.54	3.34		82.19	
WSe ₂	3.31	2.55	3.39			83.07
MoSe ₂ /WSe ₂	3.29	2.53	3.35/3.37	3.22	82.55	82.84

TABLE I. Calculated values of MX_2 single layer 2D, lattice constants, a , bond lengths, d_{M-X} and d_{X-X} in angstrom (Å), and bond angles in degree.

Because MoSe₂ and WSe₂ are polar materials, non-analytic part of the dynamical matrix which contains the effective charges and the dielectric tensor are taken into account to obtain the correct frequencies at the zone center. Indeed, certain IR-active mode (polar mode) at the zone-center give rise to a macroscopic electric field which impacts the longitudinal optical (LO) phonons in the limit of long-wavelength, breaking the degeneracy of the LO mode with the transversal optical (TO) mode.³³ The LO-TO splitting for the E' arises from the coupling of the lattice to the macroscopic electric field created by the relative displacement of Mo, W atoms and Se atoms in the long-wavelength limit.^{34,35}

III. PHONON DISPERSION

Phonons play a key role in a wide range of phenomena in condensed matter physics. For instance the major contributions of lattice thermal conductivity³⁶ and electron-phonon coupling depend on

Mode	Activity	WSe ₂				MoSe ₂			
		Cal	Ref ⁵⁰	Ref ²⁸	Exp ⁴⁴	Cal	Ref ⁵⁰	Ref ²⁸	Exp ⁵¹
E''	R	164.9	168.11	166	-	161.8	161.77	160	-
A'_1	R	236.6	241.50	241	248	234.2	236.16	233	241
E'	I+R	234.7(234.8)	238.49	238	249	276.9(279.8)	277.85	277	287
A''_2	I	293.5	298.53	298	-	342.5	342.90	343	-

TABLE II. Zone-center phonon modes of monolayers MoSe₂ and WSe₂.

phonons.^{37,38} Recently several studies have been devoted to studying the vibrational properties of graphene^{39–41}, graphene/TMDs heterostructures^{42,43}, transition metal dichalcogenides (TMDs)^{28,34,38,44–49}, and their stacked heterostructures.^{38,48} The observation of arising inter-layer phonon modes^{38,41,47,48} in van der Waals heterostructures is relevant because describe the interaction between layers. Here, we explore MoSe₂/WSe₂ vdW heterobilayer, focusing on the way the intrinsic vibrational properties of the building blocks are modified upon stacking.

A. Individual Layers

The phonon dispersions at zero stress along the main symmetry directions and its density of states (DOS) are shown in Figs.2 (a),(b). Overall, the MoSe₂ and WSe₂ phonon dispersions share a resemblance. It is worth noting the absence of degeneracies at the high-symmetry points M and K and the crossing of the LA and ZA branches just before the M point. The most relevant phonon frequencies at Γ with their character, involved atoms, and displacement direction are summarized in Table II. We shall emphasize the good agreement between our calculated dispersion and those available in the literature^{52,53}.

At the Γ point both MoSe₂ and WSe₂ possess the factor group $P-6m2$ (D_{3h} in Schönflies notation) with no center of inversion. The zone-center vibrational modes can be decomposed according to the following equation^{49,54}

$$\Gamma = A''_2 \oplus 2E' \oplus 2E'' \oplus A'_1 \oplus 2E' \oplus A''_2$$

The superscripts ' and '' represent modes that are symmetric or anti-symmetric with respect to the horizontal plane σ_h . The subscripts 1 and 2 refer to modes that are symmetric or anti-symmetric to C_2 perpendicular to principal axis C_n or vertical plane σ_v or σ_d . Furthermore, the symbol E represents the doubly degenerate vibratory modes while the symbol A stands for the non-degenerate vibratory modes.

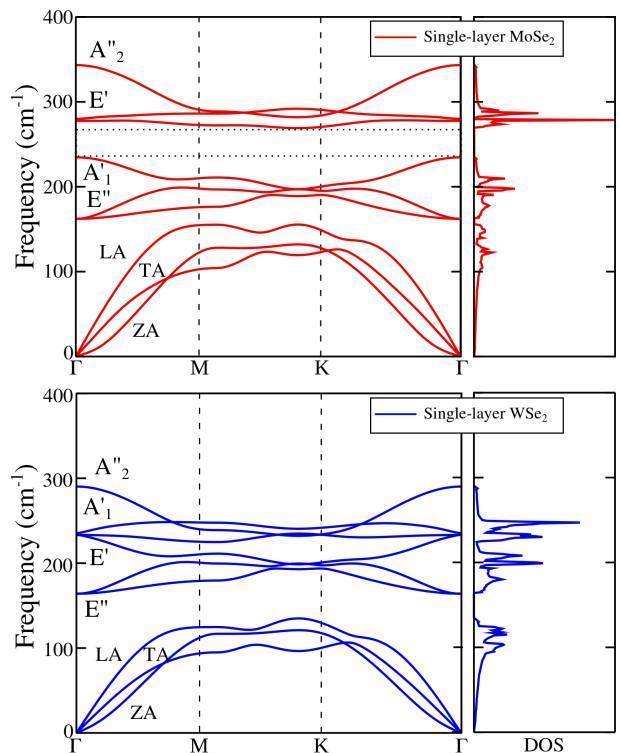


FIG. 2. (Color online) Phonon dispersion and phonon DOS for monolayer MoSe₂ and WSe₂.

The three acoustic modes are either IR-active or Raman active and can be decomposed into irreducible representations

$$\Gamma^{acoustic} = A''_2 \oplus 2E'$$

A degenerate E' mode which is divided into in-plane transversal E' TA and longitudinal E' LA mode that are both Raman and IR-active involves in-plane motions of atoms. Both LA and TA modes show linear dispersion in the long wavelength limit. The calculated LA and TA sound velocities are extracted from the slope of the acoustic branches. We obtain 4.71 (4.33) km/s and 2.91 (2.77) km/s for the LA and the in-plane TA branches, respectively in the Γ –M direction. The values between round brackets stand for WSe₂. In the direction Γ –K both values are slightly lower by about 1.4% (0.7%) for TA phonon branch and 7% (1.9%) for LA phonon branch than the ones obtained in the direction Γ –M. Such a direction dependency of the phonon propagation velocity has not been reported so far. It may have a big impact on physical properties that are related the sound velocity such as the elastic constants, in-plane stiffness, and shear modulus.

The mode A''_2 that is IR-active belongs to the out-of-plane mode ZA where the atoms move out of the plane. ZA phonons are nonlinear with respect to the wave vector with an approximate quadratic q^2 dependence as a consequence of the group symmetry. These flexural modes are particularly important for low-dimensional layered

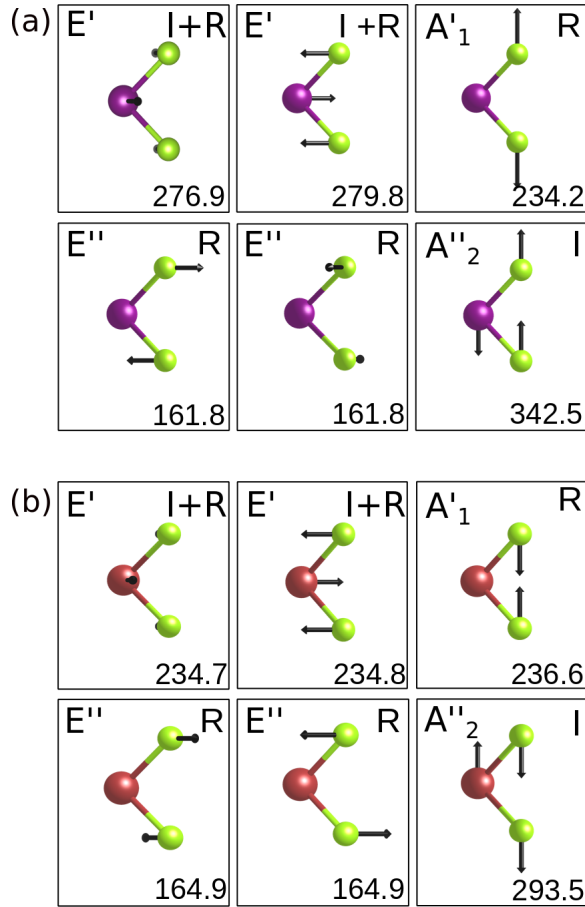


FIG. 3. (Color online) Atomic displacements for optical phonon modes of monolayers MoSe₂ (a) and (b) WSe₂.

systems^{55,56} as they have a huge contribution to the phonon DOS and are responsible for the large thermal conductance. It was also reported that the transport due to the flexural excitations is almost ballistic.³⁸ Fitting the frequencies below 40 cm⁻¹ to a parabolic function $\omega = \delta q^2$, a value of $\delta \approx 5.667 \times 10^{-7} \text{ m}^2 \text{ s}^{-1}$ and $5.648 \times 10^{-7} \text{ m}^2 \text{ s}^{-1}$ is obtained for MoSe₂ and WSe₂, respectively, which values are comparable to that of graphene ($\approx 6 \times 10^{-7}$)^{57,58}.

Finally, using the q^2 behaviour of the ZA branch we have estimated the energy necessary to roll up the MoSe₂ and WSe₂ sheet to form the tubules. To do so, we used the equation of strain energy per X–Se atom pair $E_{st} = A/r^2$ where $A = \delta^2(m_X + m_{Se})/2$, being $(m_X + m_{Se})$ the mass of the X–Se pair and r the tube radius. The value obtained for A is 5.13 eV Å²/pair and 7.86 eV Å²/pair for MoSe₂ and WSe₂, respectively, which are in the same magnitude as compared to the calculated constant for graphene and carbone nanotubes⁵⁷.

The optical zone-center modes are decomposed into

$$\Gamma^{optical} = 2E'' \oplus A'_1 \oplus 2E' \oplus A''_2$$

The eigenvectors and frequencies for the optically allowed Γ -point vibrations are shown in Fig.3. The dou-

bly degenerate E'' Raman-active modes LO₁ and TO₁ at 161.8 cm⁻¹ (164.9 cm⁻¹) involve rigid shear displacements between two neighboring Se layers in the primitive cell while the metallic atoms remain frozen. The nondegenerate out-of-plane A'_1 mode ZO₂ at 234.2 cm⁻¹ (236.6 cm⁻¹) that is Raman active consists of an out-of-plane stretching for MoSe₂ and of a rigide plane compression for WSe₂.

The high-frequency optical modes are separated from the low-frequency modes by a gap of 42.6 cm⁻¹. The doubly degenerate vibratory E' mode splits into LO₂ mode at 276.9 cm⁻¹ and TO₂ at 279.8 cm⁻¹ that are both Raman and IR-infrared and involve rigid-plane shear displacements between the metallic layer and the chalcogenide layers in the primitive cell. In the case of WSe₂ single-layer the LO-TO splitting for the E' mode has the value of 0.1 cm⁻¹ which is much smaller than in the MoSe₂ single-layer.

The nondegenerate out-of-plane A''_2 mode ZO₁ at 342.5 cm⁻¹ and 293.5 cm⁻¹ for MoSe₂ and WSe₂, respectively, that is IR-active consists of an out-of-plane stretching of the metallic atoms and chalcogenide atoms. It is worth mentioning the good agreement between the calculated phonon frequencies of single-layers MoSe₂ and WSe₂ and the experimental and theoretical results (see Table II).

B. MoSe₂/WSe₂ heterobilayer

Figure 5 displays the phonon dispersions along the main symmetry directions and the phonon DOS for MoSe₂ /WSe₂ heterobilayer. Although that the phonon dispersion curve looks similar to those of the subunits, indicating the low effect of vertical stacking on phonon structures, the phonon structure of the heterobilayer is not a simple superposition of those of isolated layers. The unit cell of the heterostructure considered here contains six atoms, resulting in eighteen phonon branches. At the Γ point they possess the factor group C_{3v} (3m). The zone-center vibrational modes can be decomposed into the following irreducible representations

$$\Gamma^{HBL} = 6A_1 \oplus 12E$$

All the zone-center phonons modes are both Raman and infrared active. The three acoustic modes can be decomposed into $\Gamma^{acoustic} = A_1 \oplus 2E$ irreducible representations. In a similar way, these three branches constitute the acoustic modes ZA, TA and LA as it is quoted before in the monolayers acoustic branches.

From Fig. 5 we can see that similar to other 2D hexagonal materials⁵⁹⁻⁶¹, the longitudinal acoustic (LA) and transverse acoustic (TA) branches show linear dependence in the vicinity of the Γ point. Notice that no imaginary frequencies occur along Γ -M and Γ -K line directions for out-of-plane acoustic ZA branch indicating that the lattice is thermodynamically stable even for long-wavelength transverse thermal vibrations. The speed of sound is calculated to be about 4.79 km/s and

4.74 km/s for the LA branch in the Γ -M direction and Γ -K direction, respectively. For in-plane TA branches, the value for the sound velocity is 3.02 km/s for both Γ -M and Γ -K directions. It is worth to mention that the sound waves travel more faster through heterobilayer than in the isolated constituents. The explanation for this trend is the compression waves (longitudinal waves) that travel fastest. This type of body waves does not exist in the isolated layers.

Examination of the dispersion curve shows that the flexural modes have departed from the quadratic wave vector dispersion and the frequency is $\omega = \delta q^x$, where $x=1.44$, which value is comparable to that of graphene/MoS₂ HBL (1.45).³⁸ The departure from the q^2 behavior is an indication that the heterobilayer is less elastic than the free-standing layers.⁴¹ Fitting the frequencies to a function $\omega = \delta q^{1.44}$, a value of $\delta \approx 1.977 \times 10^{-7} m^2 s^{-1}$ is obtained for MoSe₂ / WSe₂ heterobilayer, which values are lower than that of isolated layers confirming again the transition from an elastic systems to less elastic system.

Besides the three acoustic modes, there are 15 optical zone-center modes that are decomposed into

$$\Gamma^{optical} = 5A_1 \oplus 10E.$$

The optical phonon frequencies at Γ point for the heterobilayer are summarized in Table III. As it can be seen, the intrinsic phonon characteristics of the free-standing constituents are to a large extent preserved but, furthermore, it exhibits peculiar phonon modes that are not present in the individual building blocks. In other words, the stacking arrangements give rise to two types of optical phonons modes: ten subunits-like phonon (five MoSe₂-like phonons and five WSe₂-like phonons), and five hybrid-like phonons shown in Fig.6.

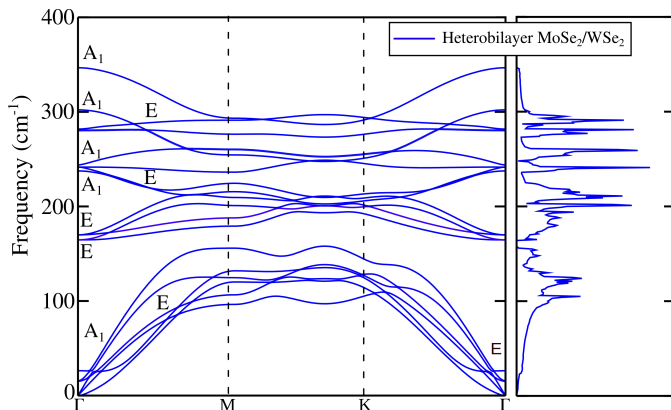


FIG. 4. (Color online) Phonon dispersion and phonon DOS of heterobilayer MoSe₂/WSe₂.

The hybrid modes also called interlayer modes can be divided into interlayer shear phonon modes (LSM) and breathing phonon modes (LBM). These vibrational modes describe the relative displacement of WSe₂ mono-

C_{3v}	Character	Type	Direction	Atoms	$\omega(\text{cm}^{-1})$
E	R + I	Interlayer	//	Mo + W + Se	15.0
A_1	R + I	Interlayer	\perp	Mo + W + Se	27.0
E	R + I	MoSe ₂ -like	//	Se	164.3
E	R + I	WSe ₂ -like	//	Se	170.4
A_1	R + I	Interlayer	\perp	Se	237.4
E	R + I	WSe ₂ -like	//	W + Se	241.8
A_1	R + I	Interlayer	//	Se	244.2
E	R + I	MoSe ₂ -like	\perp	Mo + Se	280.4
A_1	R + I	WSe ₂ -like	//	W + Se	302.3
A_1	R + I	MoSe ₂ -like	\perp	Mo + Se	346.6

TABLE III. Zone-center phonon frequencies and relevant phonon symmetry representations of heterobilayer MoSe₂/WSe₂ (point group C_{3v}). Direction // (\perp) is parallel (perpendicular) to the c vector of the unit cell, respectively.

layer with respect to the MoSe₂ monolayer in in-plane and out-of-plane directions.

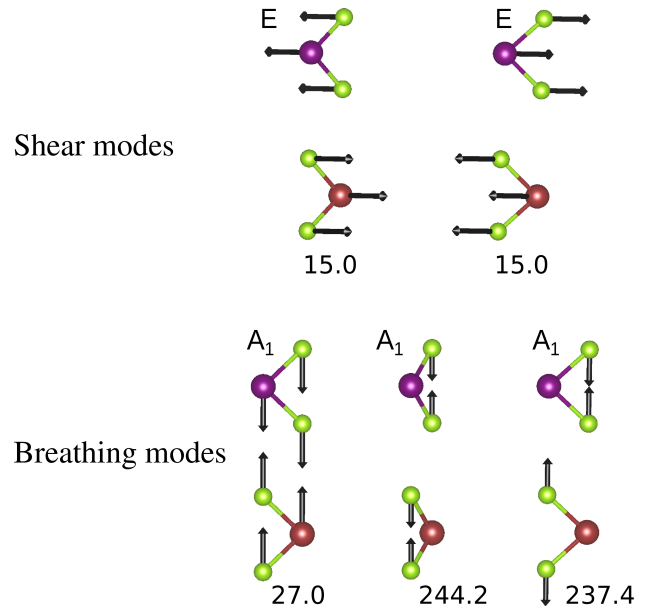


FIG. 5. (Color online) Atomic displacements for optical phonon modes of heterobilayer MoSe₂/WSe₂.

Considering the symmetry properties of the crystal, we expect two shear phonon modes and three breathing phonon modes as illustrated in Fig.6. The rigid-layer shear modes (doubly degenerate) start at 15.0 cm⁻¹ at Γ point. It is worth to notice that this mode vibration cannot be generated in the heterobilayers with incommensurate lattices because the lateral displacement of the two layers are not capable of producing any overall restoring force.⁴⁸ The frequencies of the three breathing phonon modes at the zone-center are 27, 237.4 and 244.2 cm⁻¹. Note that when the wave number \mathbf{q} increases, the acoustic and low-frequency breathing mode branches almost

match being analogous with the low-frequency optical modes of bulk MoSe₂ and WSe₂ structures. The LBM occurs only in bilayers with clean interface and are very sensitive to the vdW interactions and the relative orientation of the two monolayers.⁴⁸ They are expected to play an important role in the formation of indirect interlayer excitons in vdW heterostructures.^{18,62} Furthermore, the understanding of this kind of phonon modes provides access to the interlayer interaction and to the type of the stacking arrangement as well. Note that the frequencies of the breathing phonon modes are larger than that of the shear phonon modes. The calculated phonon dispersion (see Fig.5) shows that the energy acoustic modes of the isolated constituents did not change mostly upon stacking indicating that the MoSe₂/WSe₂ heterobilayer exhibits a thermal transport comparable to the ones of free-standing constituents. However, the thermal conductance could be deteriorated through acoustic-optical phonon scattering mechanisms involving low-frequency optical branches. The deviation of the flexural modes from characteristic quadratic dependence and the rise of interlayer modes may be very useful to unravel further fundamental properties of the heterobilayer.

IV. CONCLUSIONS

In conclusion, we have studied the structural and vibrational properties of MoSe₂/WSe₂ single layers and

their van der Waals heterobilayer MoSe₂/WSe₂ using advanced state-of-art first-principles calculations based on density functional perturbation theory and density functional theory. We find that the flexural modes have departed from quadratic wave vector characteristic of the isolated constituents. Furthermore, our calculations show the presence of interlayer shear and breathing phonon modes. The understanding of the behaviour of the vibrational properties allow us to controlling and monitoring the heat transfer in layered 2D materials.

V. ACKNOWLEDGMENTS

This work has been supported by the Algerian Ministry of High Education and Scientific Research under the PNE programme. The authors are grateful to J. Fernández-Rossier for his outstanding help and valuable advice. F. M. thanks the hospitality of the Departamento de Física Aplicada at the Universidad de Alicante. A. M.-S. acknowledges the Ramón y Cajal programme (grant RYC2018-024024-I; MINECO, Spain) and the Marie-Curie-COFUND program Nano TRAIN For Growth II (Grant Agreement 713640). *Ab initio* simulations were performed on the Tirant III cluster of the Servei d'Informàtica of the University of Valencia and on the plateforme de Calcul intensif -HPC Ibnkhaldoun of the University of Biskra.

-
- ¹ K. S. Novoselov, A. K. Geim, S. V. Morozov, D. Jiang, Y. Zhang, S. V. Dubonos, I. V. Grigorieva, and A. A. Firsov, *Science* **306**, 666 (2004).
- ² K. S. Novoselov, D. Jiang, F. Schedin, T. J. Booth, V. V. Khotkevich, S. V. Morozov, and A. K. Geim, *Proceedings of the National Academy of Sciences* **102**, 10451 (2005).
- ³ J. N. Coleman, M. Lotya, A. O'Neill, S. D. Bergin, P. J. King, U. Khan, K. Young, A. Gaucher, S. De, R. J. Smith, I. V. Shvets, S. K. Arora, G. Stanton, H.-Y. Kim, K. Lee, G. T. Kim, G. S. Duesberg, T. Hallam, J. J. Boland, J. J. Wang, J. F. Donegan, J. C. Grunlan, G. Moriarty, A. Shmeliov, R. J. Nicholls, J. M. Perkins, E. M. Grieverson, K. Theuwissen, D. W. McComb, P. D. Nellist, and V. Nicolosi, *Science* **331**, 568 (2011).
- ⁴ F. Xia, H. Wang, D. Xiao, M. Dubey, and A. Ramasubramanian, *Nature Photonics* **8**, 899 (2014).
- ⁵ H. Fang, S. Chuang, T. C. Chang, K. Takei, T. Takahashi, and A. Javey, *Nano Letters* **12**, 3788 (2012).
- ⁶ J.-K. Huang, J. Pu, C.-L. Hsu, M.-H. Chiu, Z.-Y. Juang, Y.-H. Chang, W.-H. Chang, Y. Iwasa, T. Takenobu, and L.-J. Li, *ACS Nano* **8**, 923 (2014).
- ⁷ S. Larentis, B. Fallahzad, and E. Tutuc, *Applied Physics Letters* **101** (2012), 10.1063/1.4768218.
- ⁸ S. Tongay, J. Zhou, C. Ataca, K. Lo, T. S. Matthews, J. Li, C. Grossman, and J. Wu, , 8 (2012).
- ⁹ D. Jariwala, V. K. Sangwan, L. J. Lauhon, T. J. Marks, and M. C. Hersam, *ACS nano* **8**, 1102 (2014).
- ¹⁰ A. Krasnok, S. Lepeshov, and A. Alú, *Opt. Express* **26**, 15972 (2018).
- ¹¹ A. K. Geim and I. V. Grigorieva, *Nature* **499**, 419 (2013).
- ¹² Y. Gong, S. Lei, G. Ye, B. Li, Y. He, K. Keyshar, X. Zhang, Q. Wang, J. Lou, Z. Liu, R. Vajtai, W. Zhou, and P. M. Ajayan, *Nano Letters* **15**, 6135 (2015).
- ¹³ C. H. Lee, G. H. Lee, A. M. Van Der Zande, W. Chen, Y. Li, M. Han, X. Cui, G. Arefe, C. Nuckolls, T. F. Heinz, J. Guo, J. Hone, and P. Kim, *Nature Nanotechnology* **9**, 676 (2014).
- ¹⁴ G. H. Lee, Y. J. Yu, X. Cui, N. Petrone, C. H. Lee, M. S. Choi, D. Y. Lee, C. Lee, W. J. Yoo, K. Watanabe, T. Taniguchi, C. Nuckolls, P. Kim, and J. Hone, *ACS Nano* **7**, 7931 (2013).
- ¹⁵ A. T. Hanbicki, H.-j. Chuang, M. R. Rosenberger, C. S. Hellberg, S. V. Sivaram, K. M. McCreary, I. I. Mazin, and B. T. Jonker, (2018), 10.1021/acsnano.8b01369.
- ¹⁶ A. F. Rigosi, H. M. Hill, Y. Li, A. Chernikov, and T. F. Heinz, *Nano Letters* **15**, 5033 (2015).
- ¹⁷ B. Miller, A. Steinhoff, B. Pano, J. Klein, F. Jahnke, A. Holleitner, and U. Wurstbauer, *Nano Letters* **17**, 5229 (2017).
- ¹⁸ R. Gillen and J. Maultzsch, *Phys. Rev. B* **97**, 165306 (2018).
- ¹⁹ E. Torun, H. P. C. Miranda, A. Molina-sánchez, and L. Wirtz, **245427**, 1 (2018).
- ²⁰ H. Zhu, C. Zhou, Y. Wu, W. Lin, W. Yang, Z. Cheng, and X. Cai, *Surface Science* **661**, 1 (2017).

- ²¹ P. Hohenberg and W. Kohn, *Phys. Rev.* **136**, B864 (1964).
- ²² W. Kohn and L. J. Sham, *Phys. Rev.* **140**, A1133 (1965).
- ²³ P. Giannozzi, S. Baroni, N. Bonini, M. Calandra, R. Car, C. Cavazzoni, D. Ceresoli, G. L. Chiarotti, M. Cococcioni, I. Dabo, A. D. Corso, S. de Gironcoli, S. Fabris, G. Fratesi, R. Gebauer, U. Gerstmann, C. Gougoussis, A. Kokalj, M. Lazzeri, L. Martin-Samos, N. Marzari, F. Mauri, R. Mazzarello, S. Paolini, A. Pasquarello, L. Paulatto, C. Sbraccia, S. Scandolo, G. Sclauzero, A. P. Seitsonen, A. Smogunov, P. Umari, and R. M. Wentzcovitch, *Journal of Physics: Condensed Matter* **21**, 395502 (2009).
- ²⁴ J. P. Perdew, K. Burke, and M. Ernzerhof, *Physical Review Letters* **77**, 3865 (1996).
- ²⁵ D. R. Hamann, *Phys. Rev. B* **88**, 085117 (2013).
- ²⁶ A. Tkatchenko and M. Scheffler, *Physical Review Letters* **102**, 6 (2009).
- ²⁷ J. D. Pack and H. J. Monkhorst, *Physical Review B* **16**, 1748 (1977).
- ²⁸ Y. Ding, Y. Wang, J. Ni, L. Shi, S. Shi, and W. Tang, *Physica B: Condensed Matter* **406**, 2254 (2011).
- ²⁹ C.-H. Chang, X. Fan, S.-H. Lin, and J.-L. Kuo, *Phys. Rev. B* **88**, 195420 (2013).
- ³⁰ A. Ramasubramanian, *Phys. Rev. B* **86**, 115409 (2012).
- ³¹ L. Debbichi, O. Eriksson, and S. Lebègue, *Physical Review B* **89**, 205311 (2014).
- ³² S. Baroni, S. de Gironcoli, A. Dal Corso, and P. Giannozzi, *Rev. Mod. Phys.* **73**, 515 (2001).
- ³³ M. Cardona and P. Y. Yu, Springer-Verlag, Berlin (1996).
- ³⁴ A. Molina-Sánchez and L. Wirtz, *Phys. Rev. B* **84**, 155413 (2011).
- ³⁵ Y. Cai, J. Lan, G. Zhang, and Y.-W. Zhang, *Phys. Rev. B* **89**, 035438 (2014).
- ³⁶ X. Liu and Y.-W. Zhang, *Chinese Physics B* **27**, 034402 (2018).
- ³⁷ C. Jin, J. Kim, J. Suh, Z. Shi, B. Chen, X. Fan, M. Kam, K. Watanabe, T. Taniguchi, S. Tongay, A. Zettl, J. Wu, and F. Wang, *Nature Physics* **13**, 127 (2017).
- ³⁸ N. B. Le, T. D. Huan, and L. M. Woods, *ACS Applied Materials & Interfaces* **8**, 6286 (2016).
- ³⁹ J.-A. Yan, W. Y. Ruan, and M. Y. Chou, *Phys. Rev. B* **77**, 125401 (2008).
- ⁴⁰ H. Wang, Y. Wang, X. Cao, M. Feng, and G. Lan, *Journal of Raman Spectroscopy* **40**, 1791 (2009).
- ⁴¹ C. H. Lui and T. F. Heinz, *Phys. Rev. B* **87**, 121404 (2013).
- ⁴² S. Singh, C. Espejo, and A. H. Romero, *Phys. Rev. B* **98**, 155309 (2018).
- ⁴³ X. Chen, R. Meng, J. Jiang, Q. Liang, Q. Yang, C. Tan, X. Sun, S. Zhang, and T. Ren, *Phys. Chem. Chem. Phys.* **18**, 16302 (2016).
- ⁴⁴ W. Zhao, Z. Ghorannevis, K. K. Amara, J. R. Pang, M. Toh, X. Zhang, C. Kloc, P. H. Tan, and G. Eda, *Nanoscale* **5**, 9677 (2013).
- ⁴⁵ X. Luo, Y. Zhao, J. Zhang, Q. Xiong, and S. Y. Quek, *Phys. Rev. B* **88**, 075320 (2013).
- ⁴⁶ H. Tornatzky, R. Gillen, H. Uchiyama, and J. Maultzsch, *Phys. Rev. B* **99**, 144309 (2019).
- ⁴⁷ Y. Zhao, X. Luo, H. Li, J. Zhang, P. T. Araujo, C. K. Gan, J. Wu, H. Zhang, S. Y. Quek, M. S. Dresselhaus, and Q. Xiong, *Nano Letters* **13**, 1007 (2013).
- ⁴⁸ C. H. Lui, Z. Ye, C. Ji, K.-C. Chiu, C.-T. Chou, T. I. Andersen, C. Means-Shively, H. Anderson, J.-M. Wu, T. Kidd, Y.-H. Lee, and R. He, *Phys. Rev. B* **91**, 165403 (2015).
- ⁴⁹ S. Jiménez Sandoval, D. Yang, R. F. Frindt, and J. C. Irwin, *Phys. Rev. B* **44**, 3955 (1991).
- ⁵⁰ Y. Li, Y. L. Li, W. Sun, and R. Ahuja, *Computational Materials Science* **92**, 206 (2014).
- ⁵¹ S. Tongay, W. Fan, J. Kang, J. Park, U. Koldemir, J. Suh, D. S. Narang, K. Liu, J. Ji, J. Li, R. Sinclair, and J. Wu, *Nano Letters* **14**, 1 (2014).
- ⁵² P. Johari and V. B. Shenoy, *ACS Nano* **6**, 5449 (2012), pMID: 22591011, <https://doi.org/10.1021/nn301320r>.
- ⁵³ X. Hu, L. Kou, and L. Sun, *Scientific Reports* **6** (2016), 10.1038/srep31122.
- ⁵⁴ J. Ribeiro-Soares, R. M. Almeida, E. B. Barros, P. T. Araujo, M. S. Dresselhaus, L. G. Cançado, and A. Jorio, *Phys. Rev. B* **90**, 115438 (2014).
- ⁵⁵ A. J. Samuels and J. D. Carey, *ACS Applied Materials & Interfaces* **7**, 22246 (2015).
- ⁵⁶ J.-W. Jiang, B.-S. Wang, J.-S. Wang, and H. S. Park, *Journal of Physics: Condensed Matter* **27**, 083001 (2015).
- ⁵⁷ D. Sánchez-Portal, E. Artacho, J. M. Soler, A. Rubio, and P. Ordejón, *Phys. Rev. B* **59**, 12678 (1999).
- ⁵⁸ A. Lucas, P. Lambin, and R. Smalley, *Journal of Physics and Chemistry of Solids* **54**, 587 (1993).
- ⁵⁹ B. Peng, H. Zhang, H. Shao, Y. Xu, X. Zhang, and H. Zhu, *RSC Adv.* **6**, 5767 (2016).
- ⁶⁰ D. L. Nika, E. P. Pokatilov, A. S. Askerov, and A. A. Balandin, *Phys. Rev. B* **79**, 155413 (2009).
- ⁶¹ T.-H. Liu and C.-C. Chang, *Nanoscale* **7**, 10648 (2015).
- ⁶² J. Kunstmann, F. Mooshammer, P. Nagler, A. Chaves, F. Stein, N. Paradiso, G. Plechinger, C. Strunk, Christophand Schüller, G. Seifert, D. R. Reichman, and T. Korn, *Nature Physics* **14**, 801 (2018).